Journal of Catalysis 279 (2011) 103–110

Contents lists available at ScienceDirect

Journal of Catalysis

journal homepage: www.elsevier.com/locate/jcat

Surface speciation and alkane oxidation with highly dispersed Fe(III) sites on silica

Dario Prieto-Centurion, Justin M. Notestein *

Department of Chemical and Biological Engineering, Northwestern University, Evanston, IL 60202, USA

ARTICLE INFO

Article history:
Received 20 October 2010
Revised 7 January 2011
Accepted 8 January 2011

Keywords:
Isolated site
EDTA ligand
Single-site catalyst
Supported oxide
C–H bond activation

ABSTRACT

When highly dispersed, supported Fe oxides are selective alkane oxidation catalysts, but new syntheses are required to reliably produce such materials. Here, highly dispersed, supported Fe^{3+} catalysts are prepared via incipient wetness impregnation of SiO_2 with aqueous Fe complexes of ethylenediaminetetraacetic acid (FeEDTA), followed by calcination. With Na^+ countercations, UV–visible diffuse reflectance spectra are entirely below 300 nm and H_2 temperature-programmed reduction only shows reduction at ~630 °C for all loadings up to 2.15 wt%, the maximum loading for a single impregnation cycle. These characteristics indicate isolated sites not seen for $Fe(NO_3)_3$ precursors even at 0.3 wt%. NH_4^+ countercations lead to amorphous oxide oligomers and a minority species with unusual reducibility at 310 °C. Na^+ countercations produce 'single-site' behavior in adamantane oxidation using H_2O_2 with a specific turnover frequency of 9.2 ± 0.8 ks^{-1}, constant for all Fe loadings and approximately 10 times higher than that of other well-dispersed Fe/SiO_2 materials. Similar turnover frequencies are obtained when counting only the highly reducible species on the NH_4^+-derived catalyst, allowing these sites to be tentatively assigned as small, undercoordinated clusters that are both easily reduced and participate in alkane oxidation, reminiscent of Fe-exchanged MFI zeolites.

1. Introduction

The selective oxidation of alkanes is an important challenge in catalysis due to the potential for direct conversion of low-cost feedstocks, such as natural gas and naphtha, into valuable oxygenated commodity chemicals [1]. Supported Fe catalysts and, in particular, Fe-substituted MFI zeolites have attracted industrial and academic attention due to their ability to promote NO_x decomposition [2–6] and selective partial oxidation of hydrocarbons [6–8]. It is generally accepted that some form of highly dispersed, binuclear or atomically isolated Fe^{3+} species involved in the selective processes catalyzed by these materials [5,9–13].

Several studies have sought to reproduce the structures and reactivity of these substituted zeolites on different supports [14–22]. Given that specialized reagents or preparation conditions are required in some of these preparation methods [15,20], and that multiple surface structures are often formed [18,19,21], we set out to develop a route to highly dispersed, supported Fe using commonly available reactants and synthesis routes. Here, catalysts are synthesized by incipient wetness impregnation (IWI) of SiO_2 supports with aqueous, anionic Fe^{3+} complexes of ethylenediaminetetraacetic acid, (EDTA, Fig. 1) followed by oxidative heat treatment. The nature of the countercation is important, and NaFeEDTA in particular generates 'single-site' catalysts with outstanding thermal stability to agglomeration and formation of bulk Fe oxides, in strong contrast with catalysts derived from simple Fe^{3+} salts such as $Fe(NO_3)_3$. The use of this complex as a catalyst precursor has only been minimally investigated, and no reports of its use for alkane oxidation are known [17,22,23]. Dissolved FeEDTA complexes have found previous use as absorption additives for NO_x scrubbers [24,25], but the principal application of the ligand continues to be as a preservative in the food industry [26].

2. Experimental

2.1. Materials and instruments

All catalyst syntheses were performed under air at ambient conditions unless specified otherwise. All reagents were obtained from Sigma–Aldrich. SiO_2 supports were obtained from Selecto Scientific (32–63 μm particle size, 630 $m^2\ g^{-1}$) and dried at 120 °C for 12 h under ambient pressure before use. Cellulose ester dialysis membrane tubes with a molecular weight cutoff of 100–400 Da were purchased from SpectraPor and used in the purification of the Fe complexes.

Electrospray ionization mass spectrometry (ESI-MS) measurements of Fe complexes were taken with a Thermo Finnegan LCQ instrument. Specific surface areas were calculated, using the BET equation [27], from N_2 absorption isotherms obtained with a Micromeritics ASAP 2010 apparatus. All materials were degassed 8 h at 5 mTorr and ambient temperature before measurements.

* Corresponding author.
E-mail address: j-notestein@northwestern.edu (J.M. Notestein).

0021-9517/$ - see front matter © 2011 Elsevier Inc. All rights reserved.
doi:10.1016/j.jcat.2011.01.007

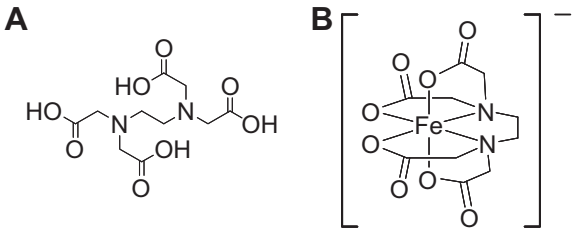

Fig. 1. Structures of (A) H_4EDTA ligand and (B) FeEDTA complex.

Elemental analysis was done using a Varian Vista MPX ICP-OES calibrated with standards of known concentration. Samples for elemental analysis were prepared by dissolving ~20 mg solids in 1 mL HF, followed by dilution to 100 mL in H_2O. Diffuse reflectance UV–visible (DRUV–vis) spectra were recorded with a Shimadzu 3600 UV–visible NIR spectrometer fitted with a Harrick Praying Mantis diffuse reflection attachment and using polytetrafluoroethylene (PTFE) as the baseline standard. All materials were thoroughly ground before acquiring spectra, and all diffuse reflectance spectra were converted to pseudo-absorption using the Kubelka–Munk transform [28,29]. Solution UV–vis measurements were performed with a standard 1-cm pathlength quartz cell. Thermogravimetric analyses (TGA) were performed in a TA Instruments Q500 thermogravimetric analyzer with an evolved gas analysis furnace. Adamantane oxidation reaction products were quantified by gas chromatography (GC) using a Shimadzu 2010 GC/FID system equipped with a Thermo-Nicolet TR-1 capillary column and compared to standards of known concentration of adamantane, and the expected products, 1-adamantanol, 2-adamantanol, and 2-adamantanone. Material balances, defined as sum of these products vs. the conversion of adamantane, were between 85% and 95% in all cases using only these products. The lower values are obtained with low Fe-loaded catalysts at low conversion and are thus attributed to the limits of instrumental precision.

For temperature-programmed reduction (TPR) experiments, the TA Q500 was fitted with a dilute H_2 feed (4.5% H_2, 4.5% Ar, and 91% He) and H_2O evolution was recorded with a Pfeiffer Thermostar Q200 mass spectrometer connected to the furnace exhaust by a fused SiO_2 capillary column maintained at 200 °C. The evolved m/z = 18 signal was calibrated against CuO reduction using Ar as the internal standard. Before TPR measurements were taken, the TA Q500 furnace was purged with UHP He for at least 90 min to remove O_2.

X-ray photoelectron spectroscopy (XPS) was performed with an Omicron ESCA probe equipped with EA125 energy analyzer. Photoemission was stimulated by a monochromated Al Kα radiation (1486.6 eV) with the operating power of 300 W. Survey scan and high-resolution scan were collected using pass energies of 50 and 25 eV, respectively. Binding energies of spectra were referenced to the C 1s binding energy set at 284.8 eV. Prior to XPS measurement, the powder samples were degassed in the entry-load chamber for 12 h.

2.2. NaFeEDTA and NH_4FeEDTA synthesis

The preparation of *monosodium Fe(III)ethylenediaminetetraacetic acid*, or NaFeEDTA, and *ammonium Fe(III)ethylenediaminetetraacetic acid*, or NH_4FeEDTA, was adapted from that described by Meier and Heinemann [30]. A two-neck round-bottom flask was charged with 10 mmol H_4EDTA, 10 mmol of $Fe(NO_3)_3{\cdot}9H_2O$, 25 mL of H_2O and heated to 60 °C with vigorous stirring under N_2 atmosphere. Once the solids fully dissolved, 40 mmol of $NaHCO_3$ or NH_4HCO_3 was slowly added. NaFeEDTA precipitated as a yellow salt within minutes, while NH_4FeEDTA solution was reduced by rotary evaporation to 4 mL to precipitate out the product. The precipitates were filtered, redissolved in water, and purified by membrane dialysis. The purified yellow solids were washed with acetone and dried under dynamic vacuum (20 mTorr) for 12 h. NaFeEDTA and NH_4FeEDTA were also prepared from $FeCl_3$ following identical procedures. ESI-MS (negative ion mode) shows m/z = 346 as the most prominent species, corresponding to the FeEDTA anion. TGA between 200 °C and 800 °C of NaFeEDTA and NH_4FeEDTA gave a mass loss due to combustion corresponding to 98.2% and 99.9% purity, respectively, according to the ratio of organic to inorganic components (Fig. S1).

2.3. Catalyst preparation

Fe was deposited on SiO_2 by IWI with aqueous solutions of NaFeEDTA and NH_4FeEDTA. The impregnated supports were stored in partially covered containers and dried 48 h at room temperature under ambient conditions, followed by 12 h under dynamic vacuum (~20 mTorr) also at room temperature. The dried materials subsequently underwent heat treatment under UHP O_2 with a ramp rate of 10 °C min^{-1} from room temperature to 800 °C, 600 °C or 400 °C. The Fe loading, expressed as Fe surface density, was varied in the range 0.05–0.65 atom nm^{-2} for NH_4FeEDTA/SiO_2 and 0.05–0.36 atom nm^{-2} for NaFeEDTA/SiO_2 (Table 1). The higher solubility of NH_4FeEDTA (>200 g L^{-1}) relative to NaFeEDTA (~100 g L^{-1}) accounts for the higher loadings obtained with the former. The highest loadings were prepared using nearly saturated solutions and thus may be subject to spontaneous precipitation

Table 1
Characteristics of the catalysts prepared for this study.

Catalyst	Fe loading[a]		
	wt%	μmol g^{-1}	atom-nm^{-2}
NaFeEDTA/SiO_2	0.30	55	0.05
[b]	0.58	103	0.10
	0.78	140	0.13
[b]	0.97	174	0.16
	1.23	221	0.21
	1.57	282	0.27
[b]	1.81	323	0.31
	2.15	384	0.36
[c]	2.15	384	0.36
[d]	2.15	384	0.36
[e]	0.91	163	0.16
NH_4FeEDTA/SiO_2	0.31	56	0.05
[b]	0.58	103	0.10
	0.75	135	0.13
[b]	0.98	175	0.17
	1.25	223	0.21
	1.57	281	0.27
[b]	1.83	331	0.31
	2.59	463	0.44
	3.25	582	0.55
	3.85	689	0.65
[c]	1.25	175	0.17
[d]	1.25	175	0.17
[e]	0.92	165	0.16
$Fe(NO_3)_3/SiO_2$	0.67	364	0.34
	1.37	244	0.23
	2.04	120	0.11
Fe_2O_3/SiO_2	1.34	240	0.23

[a] Fe wt% from amount added during IWI. Molar loadings for EDTA catalysts calculated from TGA weight losses during heat treatment agree to within 1% of those calculated from Fe added during IWI. Surface densities calculated from initial surface area.
[b] Indicates Fe loadings confirmed by ICP-OES.
[c] Heat treated to 600 °C.
[d] Heat treated to 400 °C.
[e] FeEDTA prepared from $FeCl_3$, not $Fe(NO_3)_3$.

under deposition conditions. Under typical deposition conditions, transmission UV–visible spectra of the solution showed no indication of dimeric FeEDTA complexes with characteristic absorption peaks at 475 nm [31]. Transmission electron microscopy and electron diffraction of the heat-treated materials showed no regions of high contrast or crystallinity. Transmission FT-IR spectroscopy of pressed pellets showed no significant differences between the support and heat-treated materials (Fig. S2). These negative results are expected from the low Fe loadings of these samples.

Control catalysts were prepared through IWI of SiO_2 with aqueous $Fe(NO_3)_3{\cdot}H_2O$ and through mechanical mixing of Fe_2O_3 with SiO_2 (Table 1).

2.4. Catalytic reactions

A 50-mL round-bottom flask fitted with a Liebig condenser was charged with 50 mg of catalyst, 70 mg (0.51 mmol) of adamantane, and 20 mL of acetonitrile (MeCN). The mixture was heated to 60 °C, stirred vigorously to dissolve adamantane, and 1 mL aqueous 30% H_2O_2 (9.5 mmol) was injected. Aliquots of 0.3 mL were sampled at fixed time intervals by syringe, passed through Whatman glass microfiber syringe filters with 0.7 μm pore size before being analyzed by GC-FID. The concentration of reaction products, 1-adamantanol (1-ADL), 2-adamantanol (2-ADL), and 2-adamantanone (2-ADN), was calibrated with respect to authentic standards of known concentration. Ag powder was added to each GC analysis vial to decompose any residual H_2O_2, which under GC inlet conditions potentially could further oxidize the products. Controls showed no change to product concentrations with this treatment.

3. Results and discussion

3.1. Physical characterization

N_2 physisorption of as-prepared NH_4FeEDTA and NaFeEDTA show linear loss of surface area with loading, giving a constant surface area loss of ~0.66 nm^2 per Fe complex (Fig. 2), consistent with the dimensions of the complex given elsewhere [30]. The constant loss of surface area per unit of FeEDTA indicates that for the loading range under study, the Fe complexes are not forming multilayers. This result suggests that complexing the Fe atoms with the EDTA ligand has the intended effect of preventing site aggregation by limiting metal–metal and metal–surface interactions.

TGA of the as-synthesized Fe-containing materials shows a one-step decomposition of the EDTA ligand at 240 °C, similar to that of pure H_4EDTA (Fig. S3). The loading of FeEDTA complex is determined by assuming that any mass loss between 200 °C and 800 °C in excess of that observed for the bare SiO_2 support corresponds to ligand combustion leaving $NaFeO_4$ and FeO_4 on the surface for NaFeEDTA and NH_4FeEDTA, respectively (Fig. S4). The loadings of selected materials were confirmed by ICP-OES (marked with b, Table 1).

3.2. Diffuse reflectance UV–visible spectrometry

The UV–vis absorption spectrum of the FeEDTA complex in aqueous solution shows a characteristic ligand-to-metal charge transfer (LMCT) peak at 280 nm. A similar peak is also present in the diffuse reflectance spectra of the as-made catalysts, suggesting that the complex maintains its structural integrity after impregnation. (Fig. S5) The identity of the countercation, Na^+ or NH_4^+, does not alter the shape or location of this peak.

Initial evidence for the high dispersion of the Fe atoms on the SiO_2 support can be obtained by visual inspection of the heat-treated catalysts – a red tint indicates the presence of Fe_2O_3 aggregates, while colorless materials are indicative of well-dispersed, isolated Fe^{3+} ions [15]. As Fig. 3 shows, after heat treatment, materials obtained by impregnation of NaFeEDTA remain colorless up to the maximum Fe loading of 0.36 atom nm^{-2}, whereas those obtained by impregnation of NH_4FeEDTA show a red tint for all loadings. Catalysts obtained by $Fe(NO_3)_3$ IWI are substantially darker at all loadings.

The DRUV–vis spectra of the heat-treated catalysts corroborate these initial observations. As generally agreed in the literature [14–16,18–20], isolated Fe sites absorb below 300 nm, two-dimensional amorphous oligomers absorb in the 300–500 nm range, and three-dimensional Fe_2O_3 particles absorb above 500 nm. As shown in Fig. 4A, the spectra of catalysts obtained by IWI with NaFeEDTA heat treated to 800 °C are dominated by a single well-defined peak

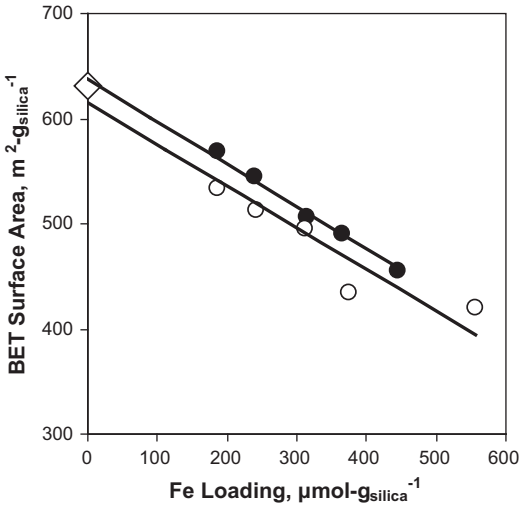

Fig. 2. Linear loss of catalyst surface area with increasing Fe loading for SiO_2 (◇) impregnated with aqueous NaFeEDTA (●) and NH_4FeEDTA. (○) The linear loss of surface area (0.66 nm^2 per Fe complex) indicates that FeEDTA complexes do not form multilayers on the SiO_2 surface.

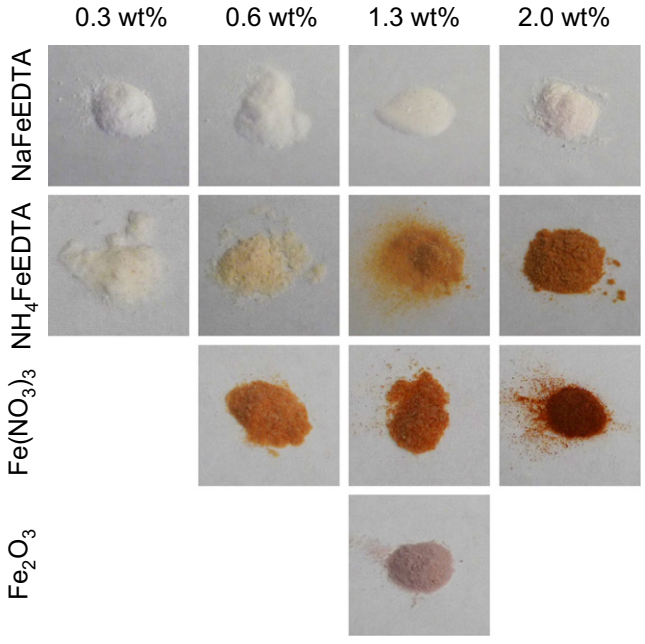

Fig. 3. Catalysts made by IWI of SiO_2 with aqueous NaFeEDTA, NH_4FeEDTA, and $Fe(NO_3)_3$ after oxidative heat treatment and by physical mixing of SiO_2 and Fe_2O_3. Materials with highly dispersed, isolated Fe^{3+} sites are expected to be colorless.

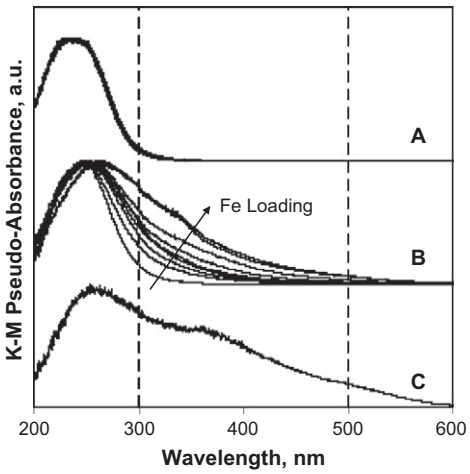

Fig. 4. DRUV–vis spectra, after oxidative heat treatment, of catalysts prepared by IWI of SiO_2 with aqueous (A) NaFeEDTA, (B) NH_4FeEDTA, and (C) $Fe(NO_3)_3$. Fe loadings are 0.30–2.15 wt%, 0.31–3.25 wt%, and 2.0 wt%, respectively. Note that for catalysts derived from NaFeEDTA, eight spectra overlay completely. Spectra are normalized to the most intense feature, but are all of similar absolute intensity.

below 300 nm. Note that eight spectra, for catalysts of Fe loadings between 0.05 and 0.36 atom nm^{-2}, are overlaid in Fig. 4A. The remarkable spectral similarity suggests that surface Fe sites in NaFeEDTA-derived materials are structurally uniform over the range of loadings under study. Furthermore, the intense peak below 300 nm can be assigned to the most intense LMCT band of very highly dispersed, 'isolated' Fe^{3+} in octahedral coordination [16]. Given that all spectra were acquired under ambient conditions, the isolated Fe^{3+} is expected to be coordinated by six oxygen atoms combined from the surface and adsorbed H_2O [15]. Coordination by H_2O after calcination at high temperature is consistent with a Lewis acidic site. The spectra of catalysts prepared by impregnation of NH_4FeEDTA possess the LMCT band below 300 nm and a tail extending beyond 300 nm which, as the Fe loading increases, becomes a prominent shoulder at 350 nm (Fig. 4B). The growing tail and shoulder can be assigned to amorphous Fe^{3+} oxide oligomers growing in nuclearity with increasing loading [16]. The much more prominent shoulder at 370 nm observed in the spectra of the heat-treated $Fe(NO_3)_3$-derived material (Fig. 4C) is also assigned to the presence of amorphous Fe^{3+} oligomers, whereas the tail extending beyond 500 nm signifies the presence of three-dimensional Fe_2O_3 crystallites [15,16]. The spectrum of mechanically mixed Fe_2O_3 and SiO_2 shows broad absorption bands of comparatively low intensity at wavelengths higher than 500 nm, indicating that most of the Fe is in a bulk oxide phase, as expected. Varying the initial heat treatment temperature did not significantly alter the spectra of any of these materials.

3.3. Temperature-programmed reduction

While DRUV–vis provides information on the presence of different oxidic Fe species, their unknown extinction coefficients preclude quantitative observations. However, the degree of dispersion is also correlated with the redox properties of the supported metal. Low-nuclearity species are generally considered to interact strongly with the support and have high reduction temperatures, while the opposite is expected of high nuclearity species [15]. Fig. 5 shows the TPR profiles, normalized to the total sample weight, of the heat-treated catalysts after oxidation to 800 °C. For all catalysts prepared through IWI, TPR shows a similar ratio of evolved H_2O to Fe atoms (0.50 ± 0.04, 0.47 ± 0.03, and 0.49 ± 0.03 for NaFeEDTA, NH_4FeEDTA, and $Fe(NO_3)_3$-derived catalysts, respectively). These ratios indicate single-electron reduction of Fe^{3+} to Fe^{2+} and are consistent with metal–surface interactions that strongly inhibit the reduction of Fe^{2+} to Fe^0 [15,17,22]. Mechanically mixed Fe_2O_3 and SiO_2 shows the expected 1.52 ± 0.03 H_2O-to-Fe ratio of the bulk oxide [32].

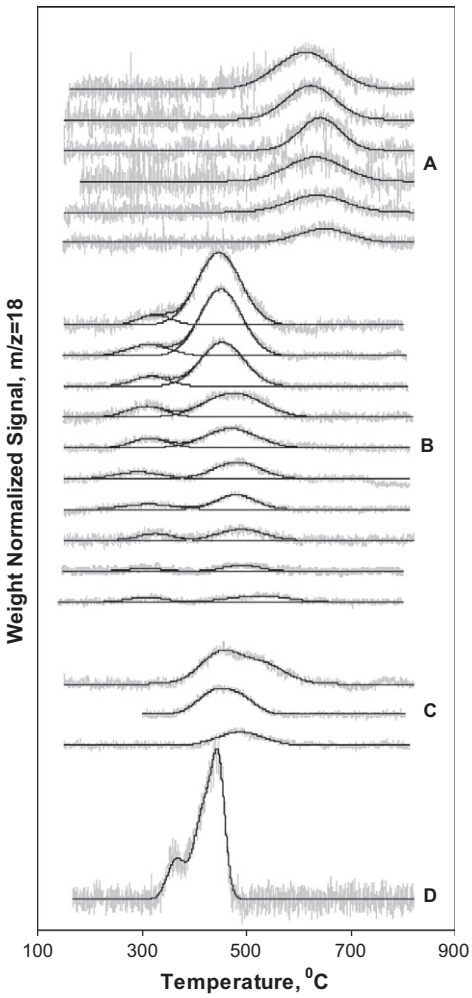

Fig. 5. TPR profiles of catalysts heat treated to 800 °C. Fe loadings increase from bottom to top within each series. SiO_2 impregnated with aqueous (A) NaFeEDTA, (B) NH_4FeEDTA, (C) $Fe(NO_3)_3$, and (D) physically mixed Fe_2O_3 in SiO_2. Profiles A show one reduction event characterized by a Gaussian peak around 630 °C. Profiles B show two reduction events characterized by Gaussian peaks around 300 °C and 500 °C. Profiles C show a single reduction event characterized by an asymmetric peak with maxima around 500 °C. Profile D shows the usual Fe_2O_3 to Fe^0 two-step transition and the expected 2:3 ratio of Fe to evolved H_2O. From profiles A, B, and C, ratios of 1:0.5 of Fe to evolved H_2O were calculated, indicating reduction from Fe^{3+} to Fe^{2+} and suggesting strong surface–metal interactions.

Catalysts prepared with NaFeEDTA show a single reduction event between 610-650 °C up to 0.36 atom nm^{-2} – the maximum Fe loading possible from a single cycle of IWI with this precursor (Fig. 5A). In contrast, catalysts prepared by the NH_4FeEDTA route show two reduction events, one between 290-320 °C and the other between 450 and 520 °C (Fig. 5B). The area under both reduction peaks initially grows proportionally to the loading, but the more reducible one plateaus at ~40 μmol H_2O per gram of catalyst, equivalent to ~80 μmol Fe per gram of catalyst or ~0.08 Fe-nm^{-2} (Fig. 6). A broad reduction event at ~500 °C is present in TPR profiles of $Fe(NO_3)_3$-derived catalysts (Fig. 5C). None of the materials prepared by IWI show the characteristic two-step reduction profile of the Fe_2O_3 powder to Fe^0 particles (Fig. 5D) [32]. The reduction temperatures identified in these catalysts are weak functions of

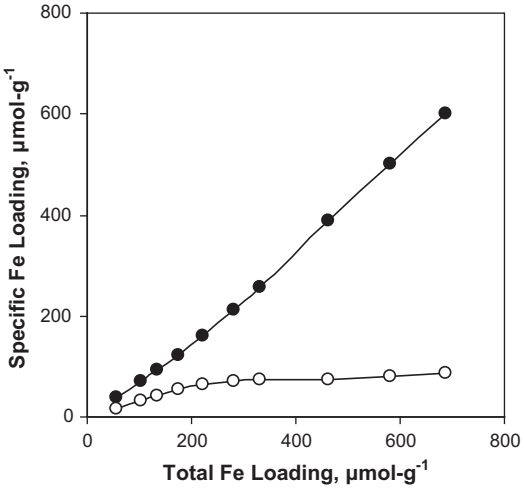

Fig. 6. Total vs. specific Fe loadings for $NH_4FeEDTA$ catalysts. The loading of the more reducible Fe^{3+} oxide species (○) plateaus near 80 µmol g^{-1} or 0.08 Fe-nm^{-2}, whereas that of the less reducible species (●) continues to grow.

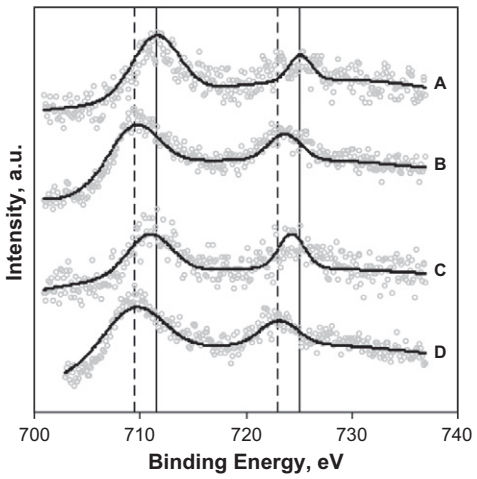

Fig. 7. X-ray photoelectron spectra of selected catalysts: 2.15 wt% Fe NaFeEDTA/SiO_2 (A) after 800 °C treatment in O_2 and (B) after 800 °C treatment in H_2, and 3.25 wt% Fe $NH_4FeEDTA/SiO_2$ (C) after 800 °C treatment in O_2 and (D) after 800 °C treatment in H_2. Solid lines at 711 and 725 eV mark the binding energy of the $2p^{3/2}$ ground state and $2p^{1/2}$ excited state, respectively, for Fe^{3+}. The broken lines at 709 and 723 eV mark the binding energy of the $2p^{3/2}$ ground state and $2p^{1/2}$ excited state, respectively, for Fe^{2+}.

loading and do not show significant variation over the studied range.

It has been reported in the literature that isolated Fe^{3+} ions undergo reduction under TPR conditions between 600 °C and 700 °C, while two-dimensional amorphous oligomers and three-dimensional crystallites reduce around 500 °C and below 400 °C, respectively [15,21]. These trends suggest that the only Fe oxide species present in the catalysts derived from NaFeEDTA are highly dispersed Fe^{3+} ions, while catalysts derived from $NH_4FeEDTA$ form predominantly amorphous two-dimensional oligomers. The other, highly reducible sites in $NH_4FeEDTA$-derived catalysts are reminiscent of Fe-exchanged MFI zeolites, some of which are known to reduce between 300 °C and 400 °C [12,13]. This similarity suggests that the reducible species be assigned as highly dispersed Fe present not as isolated atoms, but rather as very small clusters, similar to those in exchanged zeolites. The exact structure of these reducible sites synthesized via $NH_4FeEDTA$, and why they saturate at ~80 µmol Fe per gram of catalyst (~0.08 Fe-nm^{-2}), is under investigation.

Alkali metals are known to improve dispersion of transition metals on SiO_2 [33–35]. Here, Na^+ cations on the SiO_2 surface are expected to exchange with the silanolic protons upon impregnation [36]. During heat treatment, basic Na^+ ions, already tightly bound to the acidic SiO_2 surface, provide an anchor for the weakly acidic-to-amphoteric Fe^{3+} oxide which forms upon removal of the EDTA ligand. Using the EDTA complex, however, is uniquely successful in creating isolated sites because it combines the dispersion enhancement of Na^+ with the steric protection of the bulky EDTA ligand.

3.4. X-ray photoelectron spectroscopy

The quantitative TPR experiments described in Section 2.3 showed that the Fe^{3+} catalysts prepared by IWI could only be reduced to Fe^{2+} under attainable conditions. Correspondingly, XPS measurements indicate that only Fe^{3+} is present in the heat-treated catalysts, whereas Fe^{2+} is present in the reduced materials. Fig. 7 depicts the Fe 2p core level of a 0.36 atom-nm^{-2} Fe/SiO_2 derived from NaFeEDTA (A and B) and a 0.65 atom-nm^{-2} Fe/SiO_2 catalyst derived from $NH_4FeEDTA$ (C and D), after oxidation to 800 °C (A and C) and after subsequent reduction to 800 °C (B and D). The oxidized materials prepared with NaFeEDTA and $NH_4FeEDTA$ show spin-orbit splitting of the Fe $2p^{3/2}$ ground state at 711.5 eV and 711.6 eV and the Fe $2p^{1/2}$ excited state at 725.2 eV and 724.8 eV, respectively. The reduced NaFeEDTA- and $NH_4FeEDTA$-derived materials show spin-orbit splitting of $2p^{3/2}$ ground state at 709.5 eV and 709.7 eV and the Fe $2p^{1/2}$ excited state at 723.7 eV e and 723.2 eV, respectively. The peak positions and energy differences between Fe $2p^{3/2}$ and Fe $2p^{1/2}$ are typical of Fe^{3+} for the oxidized materials and Fe^{2+} for the reduced ones [37–39]. XPS measurements were taken after days of exposure to ambient conditions following reduction, and the stability of Fe^{2+} species for extended periods is indicative of strong metal–support interactions.

3.5. Oxidation of adamantane

The heat-treated materials were tested as catalysts for the oxidation of adamantane by aqueous H_2O_2 (Fig. 8). Fig. 9 shows turnover numbers (TON) for a representative catalyst (1.81 wt% Fe heat-treated NaFeEDTA/SiO_2) over 3 h (11 ks).

Adamantane is a particularly informative substrate for catalytic oxidations because the ratio of tertiary to secondary oxidation products (3°/2°) provides insight into the nature of the reaction. On a per hydrogen basis, the observed ratio of 3°/2° oxidation products after 30 min was 2.4 ± 0.1 and 2.6 ± 0.1 for catalysts derived from NaFeEDTA and $NH_4FeEDTA$, respectively. $Fe(NO_3)_3$-derived catalysts showed similar 3°/2° selectivity. In radical-mediated reactions, the lower C–H bond dissociation energy on tertiary carbons produces high 3°/2° selectivity, and some molecular Fe catalysts show values as high as 10 [40,41]. Fe salts and supported oxide catalysts typically give values between 3.7 and 2.7 [20,42,43], as observed here, indicating more reactive oxidants than the molecular catalysts, but less reactive than the largely

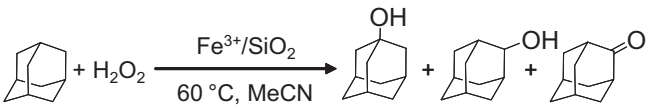

Fig. 8. Adamantane oxidation by H_2O_2 over Fe^{3+}/SiO_2. From left to right, the reaction products are 1-adamantanol (1-ADL), 2-adamantanol (2-ADL), and 2-adamantanone (2-ADN).

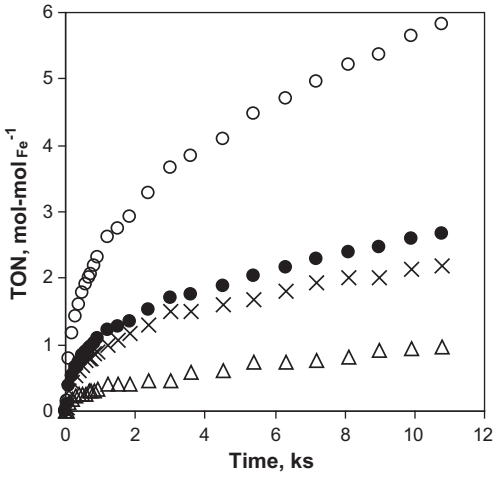

Fig. 9. Adamantane oxidation products vs. time for 1.81 wt% Fe catalysts prepared with NaFeEDTA. (○) Total TON, all reactions' products included. (●) 1-adamantanol. (×) 2-adamantanone. (Δ) 2-adamantanol.

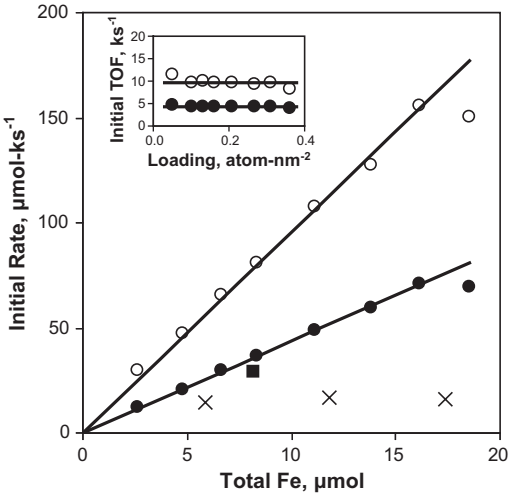

Fig. 10. Initial reaction rate vs. total Fe in reactor (21 mL solution, 50 mg catalyst) of heat-treated NaFeEDTA/SiO_2 materials for adamantane oxidation with H_2O_2. Inset: TOF in ks^{-1} vs. Fe loading in atom-nm^{-2}. Aside from small deviations for the highest and lowest loadings, the catalysts show the 'single-site' behavior expected for catalysts with uniform, highly dispersed, and equally accessible active sites. (○) Total reaction products. (●) 1-adamantanol. (×) Total reaction products over heat-treated $Fe(NO_3)_3/SiO_2$. (■) Total reaction products over heat-treated NaFeEDTA/SiO_2 made from $FeCl_3$.

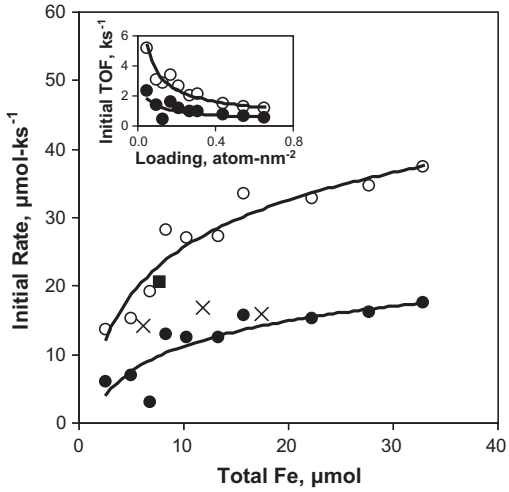

Fig. 11. Initial reaction rate vs. total Fe in reactor (21 mL solution, 50 mg catalyst) of heat-treated $NH_4FeEDTA/SiO_2$ materials for adamantane oxidation with H_2O_2. Inset: TOF in ks^{-1} vs. Fe loading in atom-nm^{-2}. The catalysts show decreasing activity per total Fe with increasing loading. (○) Total reaction products. (●) 1-adamantanol. (×) Total reaction products over heat-treated $Fe(NO_3)_3/SiO_2$. (■) Total reaction products over heat-treated $NH_4FeEDTA/SiO_2$ made from $FeCl_3$.

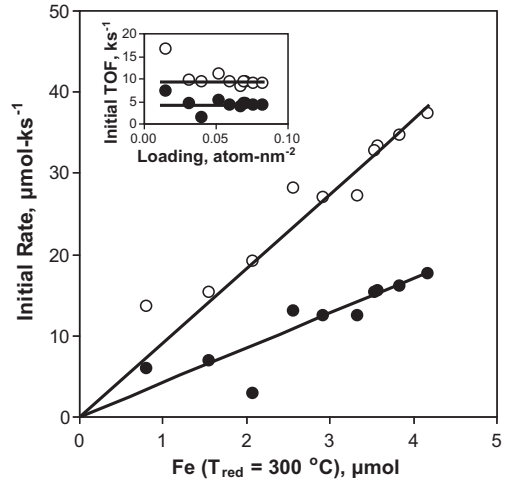

Fig. 12. Initial reaction rate vs. quantity of the more reducible Fe in reactor (21 mL solution, 50 mg catalyst) for adamantane oxidation with H_2O_2 over heat-treated $NH_4FeEDTA/SiO_2$ materials. Inset: TOF in ks^{-1} vs. Fe loading in atom-nm^{-2}. The more reducible Fe species shows 'single-site' behavior. (○) Total reaction products. (●) 1-adamantanol.

indiscriminate gas-phase OH radicals, which have an expected 3°/2° selectivity near 2 [44].

Catalysts derived from NaFeEDTA show first-order initial oxidation rates with respect to total Fe concentration (Fig. 10), or equivalently, that the initial turnover frequency (TOF) is independent of the Fe loading (Fig. 10, inset). Constant catalytic TOF is expected from the likewise-invariant DRUV–vis spectra and TPR results and suggest that Fe sites possess the same, or very similar, structures for all loadings studied. Therefore, the NaFeEDTA-derived materials are well-dispersed, site-isolated catalysts that are verifiably 'single-site'. In contrast, $Fe(NO_3)_3$-derived catalysts show much lower activity and do not show any increase in absolute rate with loading (× symbols, Fig. 10).

Catalysts derived from $NH_4FeEDTA$ show decreasing TOF (per total Fe atoms) with increasing loading (Fig. 11). This common behavior for supported oxides is consistent with a decreasing fraction of the total Fe atoms being active sites present as defects in increasingly large oxide sheets or crystallites. Although less active than NaFeEDTA catalysts, these materials still consistently show initial rates twice those of $Fe(NO_3)_3$ catalysts. However, if the initial rate is plotted against the concentration of the more reducible Fe species (those reducing between 290 °C and 320 °C) instead of the total Fe concentration, a linear relation reappears (Fig. 12). Given the low TOF of $Fe(NO_3)_3$-derived catalysts, the limiting case can be assumed, where all oxidation reactivity is ascribed to these more reducible sites in $NH_4FeEDTA$-derived catalysts. As such, the renormalized initial TOF for $NH_4FeEDTA$ catalysts, 9.3 ± 0.8 ks^{-1}, is comparable to that of the species identified in NaFeEDTA catalysts, 9.7 ± 0.2 ks^{-1}. Both are an order of magnitude larger than adamantane oxidation TOF over highly dispersed Fe-SiO_2 materials reported elsewhere [20].

The agreement between TOF on the two types of sites, and the generally high oxidation reactivity, gives further support to the hypothesis that the NH_4FeEDTA precursor generates a minority population of very small clusters, as was argued when analyzing the TPR data. Such clusters would be easily reduced due to bridging oxygens, yet also proficient in activating H_2O_2 due to the presence of undercoordinated sites. The rigorously isolated species derived from NaFeEDTA also possess undercoordinated sites capable of activating H_2O_2, but are extremely resistant to reduction. In both cases, the most highly dispersed species on each sample are proposed to be responsible for the observed oxidation catalysts. Although the pore restrictions do not permit adamantane oxidation with Fe-substituted MFI zeolites, the types of Fe active sites seen here are also considered to be responsible for high activity in oxidation with activated oxidants in Fe-substituted MFI zeolites [12,13].

3.6. Other catalytic considerations

The effect of the Fe source on the catalysts was tested by preparing catalysts with FeEDTA complexes derived from $FeCl_3$. Although Cl^- is largely removed during precursor purification, using $FeCl_3$ as the Fe source decreases the activity of NaFeEDTA noticeably, but has less of an effect for NH_4FeEDTA-derived catalysts. The NH_4FeEDTA complex is more pure, but halogen poisoning may also be less significant for the NH_4FeEDTA-derived catalysts because only a minority of the sites is proposed to be active in catalysis.

Under reaction conditions, neither isomerization of alcohols nor oxidation of 2-ADL to 2-ADN were found to occur. This result indicates that a possible reaction mechanism includes the transformation of adamantane to alkylperoxide intermediates that subsequently decompose to the product alcohols and ketones. In such cases, thermal decomposition of residual alkylhydroperoxides can skew apparent product distributions during GC analysis. Some reaction aliquots were therefore treated with triphenylphosphine (PPh_3) to reduce alkylhydroperoxides to the corresponding alcohols, in accordance with a method from the literature [45]. For the catalysts under study, treatment with PPh_3 did not alter the product distribution, indicating that alkylhydroperoxide intermediates do not reach significant concentrations under reaction conditions, although there is insufficient evidence to completely discount the formation of metal-alkylperoxide or alkylhydroperoxide species as transiently formed intermediates.

Fe leaching into solution under adamantane oxidation conditions was calculated by ICP-OES to be 0.2%, 0.4%, and 0.6% of the Fe present on the surface for catalysts heat treated at 800 °C, 600 °C, and 400 °C, respectively. Pretreatment at 800 °C was selected for the majority of the catalyst testing primarily due to its lowest level of leaching; leached Fe concentrations were 0.3 and 3.4 μM for the lowest and highest loaded catalysts, respectively. If only the Fe^{3+} in solution were active, its initial TOF would approach 3500 ks^{-1} – over 300x that ascribed to surface catalysis. However, under conditions used in this study, the homogeneous oxidation of adamantane by H_2O_2 over 180 μM Fe^{3+} from $Fe(NO_3)_3$ shows an initial TOF of 4.9 ks^{-1}, which is of the order of the initial TOF ascribed to the heterogeneous catalysts. Oxidation products could not be observed when using Fe concentrations comparable to those expected in solution under reaction conditions. Similarly, hot filtration after three minutes of reaction completely halts the reaction in solution, (Fig. S6) which is consistent with the vast majority of the reaction occurring on the catalyst surface. Likewise, the loss of a small fraction of surface Fe as leached Fe^{3+} is unlikely responsible for the observed decrease in TOF after 1000s – this would again imply unrealistically high TOF for surface Fe before they are leached. The change in TOF with time is more likely related to a reorganization of the surface FeOx under reaction conditions, which remains under investigation.

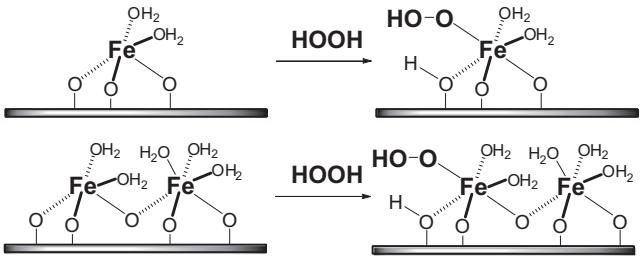

Fig. 13. (top) Atomically dispersed Fe is proposed to be formed as the sole species on catalysts derived from NaFeEDTA. (bottom) Small clusters of FeOx are proposed to be formed as a reactive minority species on catalysts derived from NH_4FeEDTA. Both types of low-nuclearity species are expected to coordinate H_2O_2 at sites left vacant by loss of H_2O or solvent. Coordinated hydroperoxide is proposed to be the first intermediate formed on route to a surface species sufficiently oxidizing to abstract H from adamantane, which then forms the observed products. In contrast to similar observed oxidation behavior, the bridging O will make the small clusters substantially more reducible in H_2 than are the atomically dispersed species.

4. Conclusions

This study demonstrates a straightforward method to create well-defined, isolated Fe sites for alkane oxidation by H_2O_2 via IWI of SiO_2 with aqueous FeEDTA complexes. The Fe dispersion attained by this method is much higher than for IWI with $Fe(NO_3)_3$, as measured by TPR and DRUV–vis spectrophotometry. NaFeEDTA is particularly effective at dispersing Fe sites, leading to rigorously 'single-site' reactivity and spectroscopic behavior, due to the combined action of the Na^+ cation and the bulky chelating ligand. Three types of surface species were identified by DRUV–vis spectrophotometry and subsequently quantified by TPR. Two-dimensional amorphous oligomers and crystallites are present for catalysts derived from $Fe(NO_3)_3$; two-dimensional oligomers are also the dominant species on the surface of NH_4FeEDTA-derived catalysts. These surface sites are poorly active in adamantane oxidation by H_2O_2. A minority of the sites in NH_4FeEDTA-derived catalysts are easily reduced and also proposed to be responsible for reactivity in adamantane oxidation, reminiscent of sites assigned as small clusters in Fe-exchanged MFI zeolites. In contrast, all of the Fe in NaFeEDTA-derived materials are assigned as isolated sites that are an order of magnitude more active than those found in other highly dispersed Fe preparations and share the same apparent TOF (9–10 ks^{-1} or 32–36 h^{-1}) as the minority sites in NH_4FeEDTA-derived catalysts. This latter finding suggests that alkane oxidation by H_2O_2 over Fe catalysts requires undercoordinated Fe found in isolated sites or small clusters, but is structure insensitive within this narrow subclass of Fe species. As illustrated in Fig. 13, very small clusters and atomically dispersed species are both expected to coordinate H_2O_2 at sites left vacant by loss of H_2O or solvent. Coordinated hydroperoxide as Fe(III)OOH is proposed as the first intermediate toward the formation of a surface species sufficiently oxidizing to abstract H from adamantane. Soluble, non-heme model complexes suggest the formation of high-valent Fe(IV) or Fe(V) oxo or oxo-hydroxo species as the oxidizing center [46], but the limits of the current study permit neither rigorous assignment of the oxidizing species nor the reaction pathway, analysis of which is in progress.

Acknowledgments

JMN acknowledges the support of Northwestern University and a 3M Non-Tenured Faculty Grant, and DPC acknowledges the

support of Patrick G. and Shirley W. Ryan through the Ryan Fellowship. XPS was performed in the Keck-II facility of NU*ANCE* Center at Northwestern University. NU*ANCE* Center is supported by NSF-NSEC, NSF-MRSEC, Keck Foundation, the State of Illinois, and Northwestern University. ICP-OES and ESI-MS were performed in the IMSERC facilities at Northwestern University with the support of the National Science Foundation under DMR-0114235.

Appendix A. Supplementary material

Supplementary data associated with this article can be found, in the online version, at doi:10.1016/j.jcat.2011.01.007.

References

[1] A.T. Bell, B.C. Gates, D. Ray, Basic research needs: catalysis for energy, in: Basic Energy Sciences Workshop, US Department of Energy, 2007.
[2] V.I. Sobolev, G.I. Panov, A.S. Kharitonov, V.N. Romannikov, A.M. Volodin, K.G. Ione, J. Catal. 139 (1993) 435–443.
[3] J. Valyon, W.S. Millman, W.K. Hall, Catal. Lett. 24 (1994) 215–225.
[4] H.-Y. Chen, W.M.H. Sachtler, Catal. Today 42 (1998) 73–83.
[5] R. Joyner, J. Phys. Chem. B 103 (1999) 5963–5976.
[6] Q. Zhu, R.M. van Teeffelen, R.A. van Santen, E.J.M. Hensen, J. Catal. 221 (2004) 575–583.
[7] V.I. Sobolev, K.A. Dubkov, O.V. Panna, G.I. Panov, Catal. Today 24 (1995) 251–252.
[8] A. Ribera, I.W.C.E. Arends, S. de Vries, J. Pérez-Ramírez, R.A. Sheldon, J. Catal. 195 (2000) 287–297.
[9] L.J. Lobree, I.-C. Hwang, J.A. Reimer, A.T. Bell, J. Catal. 186 (1999) 242–253.
[10] P. Marturano, A. Kogelbauer, R. Prins, J. Catal. 190 (2000) 460–468.
[11] A.L. Yakovlev, G.M. Zhidomirov, R.A. van Santen, J. Phys. Chem. B 105 (2001) 12297–12302.
[12] F. Heinrich, C. Schmidt, E. Löffler, M. Menzel, W. Grünert, J. Catal. 212 (2002) 157–172.
[13] M. Schwidder, M.S. Kumar, K. Klementiev, M.M. Pohl, A. Brückner, W. Grünert, J. Catal. 231 (2005) 314–330.
[14] F. Arena, F. Frusteri, L. Spadaro, A. Venuto, A. Parmaliana, Stud. Surf. Sci. Catal. vol. 143 (2000) 1097–1105.
[15] F. Arena, G. Gatti, G. Martra, S. Coluccia, L. Stievano, L. Spadaro, P. Famulari, A. Parmaliana, J. Catal. 231 (2005) 365–380.
[16] S. Bordiga, R. Buzzoni, F. Geobaldo, C. Lamberti, E. Giamello, A. Zecchina, G. Leofanti, G. Petrini, G. Tozzola, G. Vlaic, J. Catal. 158 (1996) 486–501.
[17] Z. Gabelica, A. Charmot, R. Vataj, R. Soulimane, J. Barrault, S. Valange, J. Therm. Anal. Calorim. 95 (2009) 445–454.
[18] A. Gervasini, C. Messi, P. Carniti, A. Ponti, N. Ravasio, F. Zacheria, J. Catal. 262 (2009) 224–234.
[19] A. Gervasini, C. Messi, A. Ponti, S. Canedese, N. Ravasio, J. Phys. Chem. C 112 (2008) 4635–4642.
[20] C. Nozaki, C.G. Lugmair, A.T. Bell, T.D. Tilley, J. Am. Chem. Soc. 124 (2002) 13194–13203.
[21] A. Parmaliana, F. Arena, F. Frusteri, A. Marinez-Arias, M.L. Granados, J.L. Fierro, Appl. Catal. A 226 (2002) 163–174.
[22] S. Valange, R. Palacio, A. Charmot, J. Barrault, A. Louati, Z. Gabelica, J. Mol. Catal. A: Chem. 305 (2009) 24–33.
[23] A.J. van Dillen, R.J.A.M. Terorde, D.J. Lensveld, J.W. Geus, K.P. De Jong, J. Catal. 216 (2003) 257–264.
[24] T.W. Chien, H.T. Hsueh, B.Y. Chu, H. Chu, Process Saf. Environ. Protect. 87 (2009) 300–306.
[25] L. Wang, W. Zhao, Z. Wu, Chem. Eng. J. 132 (2007) 227–232.
[26] T.E. Furia, Sequestrants in food, in: T.E. Furia (Ed.), CRC Handbook of Food Additives, CRC Press, Boca Raton, 1980, pp. 272–273.
[27] S. Brunauer, P.H. Emmett, E. Teller, J. Am. Chem. Soc. 60 (1938) 309–319.
[28] P. Kubelka, F. Munk, Z. Tech. Phys. 12 (1931) 593–601.
[29] F.C. Jentoft, in: B.C. Gates, H. Knozinger, F.C. Jentoft (Eds.), Advances in Catalysis, Academic Press, Amsterdam, 2009, pp. 141–148.
[30] R. Meier, F.W. Heinemann, Inorg. Chim. Acta 337 (2002) 317–327.
[31] G. McLendon, R.J. Motekaitis, A.E. Martell, Inorg. Chem. 15 (1976) 2306–2308.
[32] M.J. Tiernan, P.A. Barnes, G.M.B. Parkes, J. Phys. Chem. B 105 (2001) 220–228.
[33] M.A. Bañares, N.D. Spencer, M.D. Jones, I.E. Wachs, J. Catal. 146 (1994) 204–210.
[34] S. Irusta, A.J. Marchi, E.A. Lombardo, E.E. Miro, Catal. Lett. 40 (1996) 9–16.
[35] S. Yang, W. Zhu, Q. Zhang, Y. Wang, J. Catal. 254 (2008) 251–262.
[36] L.H. Allen, E. Matijevíc, L. Meites, J. Inorg. Nucl. Chem. 33 (1971) 1293–1299.
[37] R.S. Prakasham, G.S. Devi, K.R. Laxmi, C.S. Rao, J. Phys. Chem. C 111 (2007) 3842–3847.
[38] T. Herranz, S. Rojas, F.J. Pérez-Alonso, M. Ojeda, P. Terreros, J.L.G. Fierro, Appl. Catal. A 308 (2006) 19–30.
[39] Y. Joseph, G. Ketteler, C. Kuhrs, W. Ranke, W. Weiss, R. Schlogl, Phys. Chem. Chem. Phys. 3 (2001) 4141–4153.
[40] A.N. Biswas, P. Das, A. Agarwala, D. Bandyopadhyay, P. Bandyopadhyay, J. Mol. Catal. A 326 (2010) 94–98.
[41] F. Minisci, F. Fontana, S. Araneo, F. Recupero, S. Banfi, S. Quici, J. Am. Chem. Soc. 117 (1995) 226–232.
[42] G. Roelfes, M. Lubben, R. Hage, J.L. Que, B.L. Feringa, Chem. Eur. J. 6 (2000) 2152–2159.
[43] B. Singh, J.R. Long, F.F.d. Biani, D. Gatteschi, P. Stavropoulos, J. Am. Chem. Soc. 119 (1997) 7030–7047.
[44] J.K. Kochi, Free radicals, in: J.K. Kochi (Ed.), Reactive Intermediates in Organic Chemistry, Wiley, New York, 1973.
[45] G.B. Shul'pin, J. Mol. Catal. A: Chem. 189 (2002) 39–66.
[46] A. Bassan, M.R.A. Blomberg, P.E.M. Siegbahn, L. Que, J. Am. Chem. Soc. 124 (2002) 11056–11063.